PHOTO REFLECTIVITY AND PHOTO ELECTRON YIELD FROM TECHNICAL SURFACES *

A. Liedl[1†], M. Angelucci[1], E. La Francesca[1,3], F. Schäfers[2], M.G. Sertsu[2], F. Siewert[2], A. Sokolov[2] and R. Cimino[1]
[1] *LNF-INFN, 00044 Frascati, Italy*
[2] *Helmholtz-Zentrum-Berlin, 12489 Berlin, Germany*
[3] *University of Rome "La Sapienza", 00185 Rome , Italy*

Abstract

The knowledge of material properties is an essential step to design particle accelerators and High Energy Colliders. During operation of these machines, the walls of the vacuum chambers are subjected to bombardment of photons and electrons. The detrimental interactions may be followed by issues related to vacuum and beam instability. Hence, it becomes crucial to obtain experimental data about these interaction in conditions as close as possible to the operative ones. Among others properties, Reflectivity (both specular and total component) and photoyield are of particular interest. These data will be used in numerical simulations to design vacuum systems. In an experimental campaign, carried out at the OPTICS beamline of BESSYII, we investigated the Reflectivity and the Photon Yield of technical materials of interest for the High Luminosity LHC upgrade and Future Circular Collider-hh design.

INTRODUCTION

The design of vacuum systems for future charged particle accelerators must face and solve issues related to beam induced effects [1]. Particularly, the High Energy Colliders and the positively charged particles accelerators may incur into important limitations due to the Synchrotron light interaction with vacuum chambers walls. This interaction can induce gas desorption and photoelectrons from the walls surface with detrimental consequences to vacuum stability, heat load and e-cloud build up. The scientific community has developed solutions to mitigate such effects and their consequences [1] but the development of a new generation of High Energy Collider, pushing forward the characteristics of these machines (energy, performances, size), increases the impact of beam induced effects. [2]
The Future Circular Collider (FCC-hh) considers to reach an energy of 100 TeV in the center of mass operating with a up to 16 T Dipole magnet field. These objective enhances the design constraints already present in LHC such as the maintenance of superconductive temperature on the dipole walls, vacuum and beam stability. During the LHC design and development, these problems have been solved by the construction of a beam screen (BS) compliant with all these requirements. BS of LHC represents the starting point of the new FCC-hh BS design [2].
Simulations of the various solutions proposed for the BS design are the tool for the forecasting of the performances in terms of heat load, beam induced multipacting and molecular density behavior [3-4]. To simulate such phenomena, the codes need some input parameters including photon Reflectivity (R), photoyield (PY, e- produced per incident photon), secondary electron yield (SEY), photon and electron stimulated desorption (PSD and ESD) and their dependencies on photon energy distribution and angle of incidence [5-12]. Calculations, modelling the effect of these parameters on the machine performance, are often based on the assumption of ideal material surface or trying to suppose characteristic of the operating ones. We show here, that only measurements on real representative samples can give the right input parameters[9]. In this context, this work presents some results of the experimental campaign conducted at OPTICS beamline at BESSYII on different technical surfaces.

EXPERIMENTAL

OPTICS beamline at BESSYII is a dedicated laboratory for "at wavelength" metrology of x-ray optical elements, reflectometry for nondestructive characterization and depth-profiling of microstructures, layered systems and buried interlayers [13-14]. There are many techniques for characterization of surface quality and finish of optical systems (Atomic Force Microscopy, White Light Interferometry, X-ray Diffraction and others..) and at-wavelength metrology for reflectivity and diffraction efficiency represent the final test bench. OPTICS beamline has been upgraded in the last years as described in details in [15]. The average spot size at the sample is 0.2x0.3 mm^2 size with a divergence of 0.5 mrad x 3.6 mrad. These features are sufficient to avoid any significant increase of beam size up to the detector positioned 310mm further downstream. The photon beam energy interval used for the experiment ranges from 35 to 1800 eV. The lower limit was determined to avoid second or higher orders of radiation, since above 35 ev, we can use second order suppression filters. The upper limit is the result of an optimization of radiation flux, available beam time and experimental specifications. Thus, the energy range

* This work was supported by INFN National committee V trough the "MICA" project. We thank HZB for the allocation of synchrotron radiation beamtime. Research leading to these results has also received funding by the project CALIPSOplus, under the Grant Agreement 730872 from the EU Framework Programme for Research and Innovation HORIZON 2020. We thank R. Valizadeh and O. Malyshev for providing us with the LASE sample. M.A. acknowledges the support of the WP4 "EuroCirCol" project, the European Union's Horizon 2020 research and innovation programme under grant agreement No. 654305.
† andrea.liedl@lnf.infn.it

covers perfectly the HILUMI-LHC spectrum (ϵ_{cr}≈50 eV) and also a useful interval for the understanding of beam induced effects in FCC-hh (ϵ_{cr}=4.3 keV). The endstation of the beamline is the UHV-Reflectometer, equipped with a four circle goniometer: two for samples and two for the detector. Furthermore, the sample position can be adjusted by using a UHV tripod systems (six degrees of freedom) that allows the fine alignment of the sample. The resolution and the range of such movements are extremely precise and allow to work at as grazing incidence as possible close to the working SR incident angle in LHC and FCC, respectively 0.28° and 0.07°. Thus, the energy range and the geometrical conditions, provided at the end-station, guarantee the reliability of the obtained data as input for the simulation codes and indicate the necessity of specialized experimental layout for such benchmark measures. For our experiments we define:

- θ_i:as the angle of incidence between photon beam and sample surface;
- θ_r:as the detector angle that identifies the position of the detector from the optical axis;
- ϕ:as the detector off-plane position defined as the distance from the plane normal to sample surface and containing the optical axis (ϕ=0).

Downstream, a series of detectors with variable apertures, obtained by the use of different pinholes, are available as described in ref [12-14]. The use of the specialized instrumentation of the OPTICS beamline allows to measure the different optical properties. Specular Reflectivity (R) is measured in the configuration shown in Fig.1-Left. The reflected beam is collected by a 4x4mm^2 detector placed at the specular position θ_r=2θ_i. The acceptance angle of the detector is 0.37° both in θ_r and in ϕ. This large aperture ensures the detection of the specular reflected signal and also some scattered radiation by rougher surface. R was measured either keeping fixed the photon beam energy and scanning over the different incident angles, or keeping fixed the geometry and scanning over the photon beam energy. The minimum angle of incidence was determined by the length of the sample and the beam size, so can change case by case. PY is measured in the same configuration measuring the photoelectrons by the current read through a Keythley picoamperometer connected to ground. During the measurement, the sample is insulated and without any bias in order to avoid possible noise. In the same way of R, PY was measured as function of incident angles and as function of photon energy. Total Reflectivity (R_t) is measured in the configuration shown in Fig.1-Right. The reflected and scattered radiation are collected by the detector, scanning over θ_r and keeping fixed the photon energy and the incident angle. The acquisition is repeated for other two different off-plane ϕ values in the positive verse. Assuming a symmetrical behavior on the two sides of the sampe, the angular distribution of the scattered radiation over a solid angle Ω is measured and R_t is obtained by this full solid angle integration.

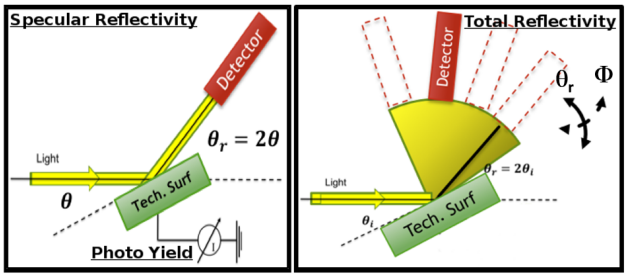

Figure 1: Two experimental configurations. (Left) $\theta/2\theta$ geometry for the measurement of R and PY keeping fixed beam energy scanning over different angles or keeping fixed geometry scanning over different beam energies. (Right) Measurement of angular distribution of reflected and scattered radiation keeping fixed beam energy and angle of incidence θ_i

SAMPLES

In this work we present results of some samples representative of materials of interest for the FCC-hh design (Fig.2). In particular we have analyzed:

- Flat Copper (Cu): Commercial Copper. Four samples distinguished by different surface treatments and different roughness (Fig.2a);
- LHC Copper (Cu-LHC): Representative sample of copper colaminated material used in LHC (Fig.2b);
- LHC Copper Saw Tooth (ST): Representative sample of copper used in the LHC with a Saw Tooth profile (40 µm high and 500µm pitch) (Fig.2c);
- Laser Treated Copper (LASE): a Representative sample of Copper treated by laser ablation process. This treatment gives to the surface particular morphology constituted by different scale structures, micrometrical grooves with coral-like sub-micron agglomeration of nano-spheres. (Fig.2d). The sample was processed at ASTeC, STFC Daresbury Laboratory, by R. Valizadeh within the WP4 EuroCirCol using the following Laser Parameters: Scan Speed 180mm/s; Power 50W: Waveform 30; Pitch 20um and Wavelength 1064nm; [16]

These four families of samples differ firstly for the roughness e for the surface aspect due to the surface treatments. The roughness was measured by the use of AFM microscopy in various metrology laboratories (HZB, CERN, INFN, CNIS-Rome1) investigating an area of 20x20 um^2. The samples Cu and Cu-LHC present similar values of R_a, respectively ≈10 nm and ≈ 15 nm, but different enough to have an impact on the optical properties. On the other hand, the design of the ST was specific to avoid the forward Reflection [17] while the LASE's hard processed surface was particularly designed for the reduction of emission of produced secondary electrons [16].

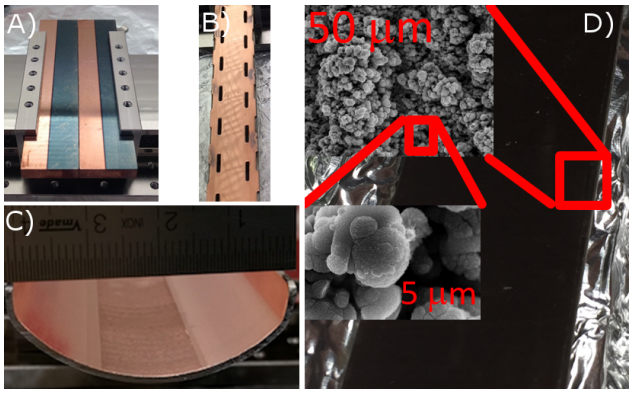

Figure 2: Investigated samples: a) Flat Copper (Cu), b) LHC Copper (Cu-LHC), c) LHC Copper Saw Tooth (ST), d) Laser Treated Copper (LASE)

RESULTS

SR metrology and experiments on real samples and in real conditions, is proved to be essential in order to provide useful input for the simulation codes during design phase of accelerators. In this section only some of the obtained results and discussions are presented. More specific and deeper analysis will be addressed in dedicated paper [18] In Fig.3, the experimental results for R are shown as a function of photon energy for three different incident angles: 0.25°, 0.5° and 1°. By a first analysis is possible to assess general features:

- R is higher for lower photon energies and at lower incident angles;
- The Cu $L_{2\text{-}3}$ absorption edge (≈930eV) is visible within the spectra as a drop of R. This feature is less evident for LASE;
- In all spectra the absorption K-edges of O and C (≈ 530eV and ≈280eV) are visible. These elements are present as contaminants on the surface;
- Values of R largely differ for the different samples. Cu and Cu-LHC present values from 0.9 to 0.3 and the low R_a of Cu implicates higher specular reflectivity. On the other hand, R for ST is always below 0.05 and below 0.01 for LASE;

Contemporary to the acquisition of R, the PY has been acquired and its dependence on the beam energy is plotted in Fig.4. Looking at the results it is possible to identify several features:

- The PY is higher for higher photon energies. The PY is strongly connected to the effective interaction with absorbed photons, hence it will be higher where R is lower;
- The PY is higher for higher incident angles. This statement is true only for a limited range of θ_i. In fact, higher incident angles generally increase the absorption and the production of photoelectrons. At the same time, beyond a certain value of θ_i the radiation penetrates too deep within the bulk and the produced photoelectrons could not be emitted. This phenomenon will be better discussed in [18];

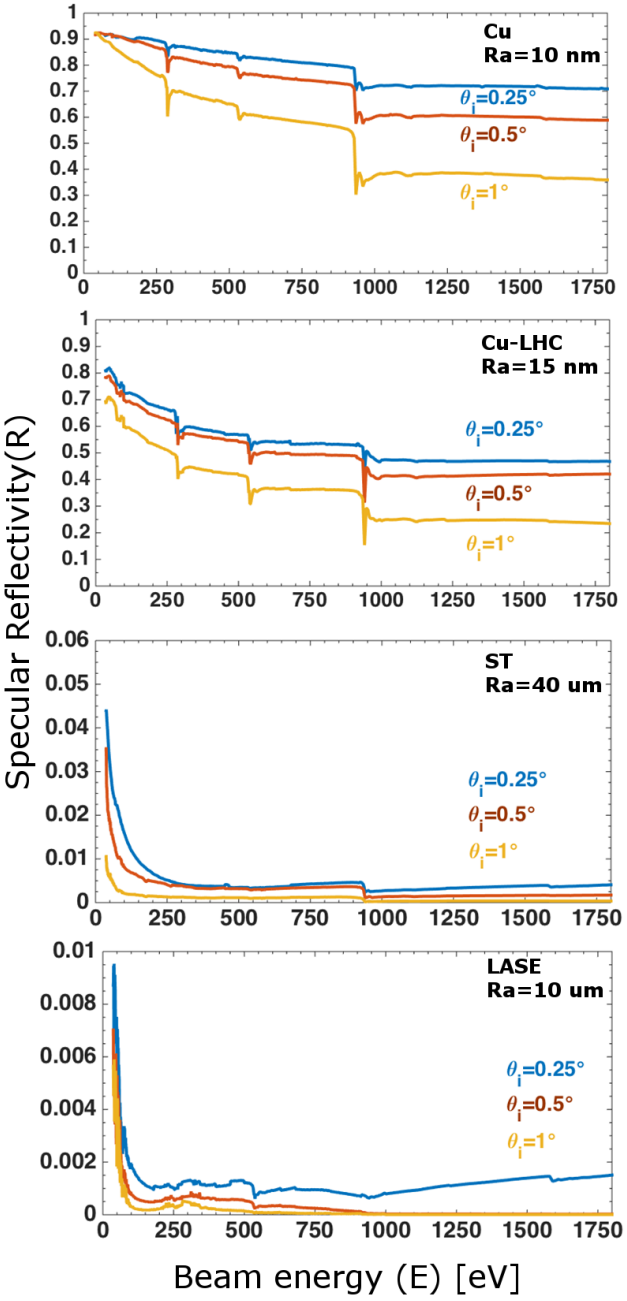

Figure 3: Specular R of different samples. From top to bottom Cu, Cu-LHC, ST and LASE

- The Cu $L_{2\text{-}3}$ absorption edge is visible and causes an increase of the PY due to the increment of the number of absorbed photons interacting with the material;
- The absorption K-edges of O and C are present. These elements are contaminant on the surface and their pres-

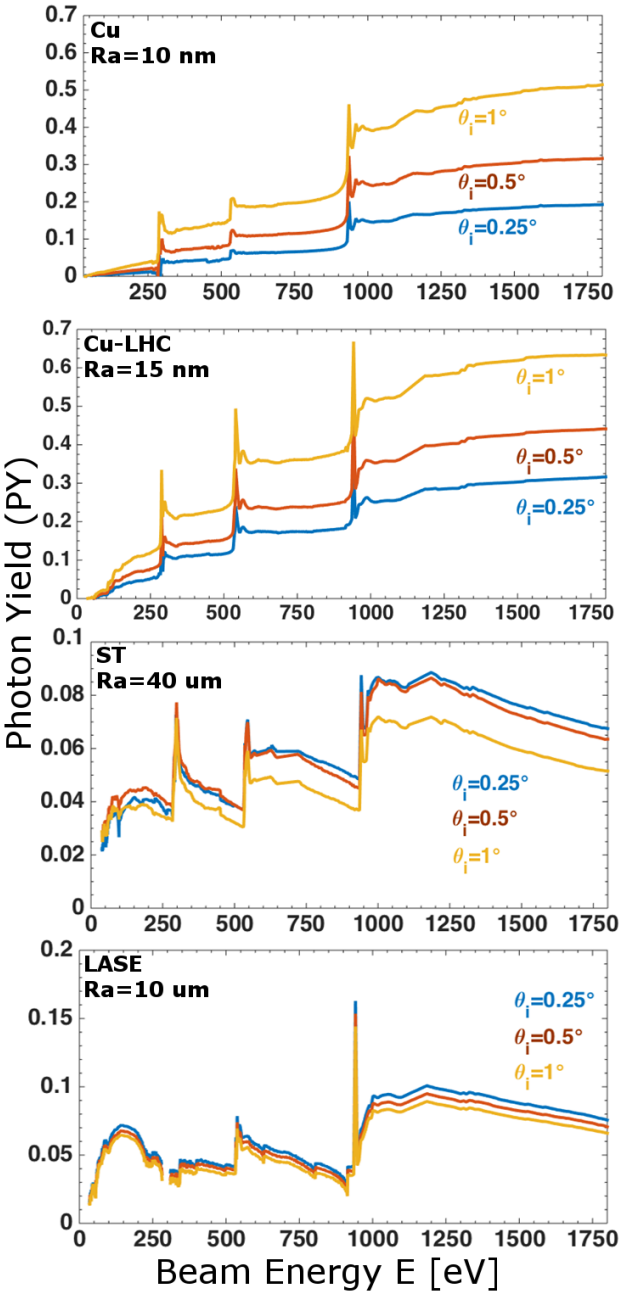

Figure 4: PY of four different samples. From top to bottom: Cu, Cu-LHC, ST and LASE

ence causes an increment of PY at the corresponding edges;

- The roughness and the surface aspect influence PY. For the moderate difference of R_a between Cu and LHC-Cu, the PY slightly changes. Otherwise, in the case of ST and LASE the PY results strongly reduced by a factor 5 or more;

The experimental results relative to the angular distribution of reflected radiation are shown in Fig.5. In particular, Fig.5 top panel is an example of angular distribution for a fixed incident angle and fixed photon energy from a Cu

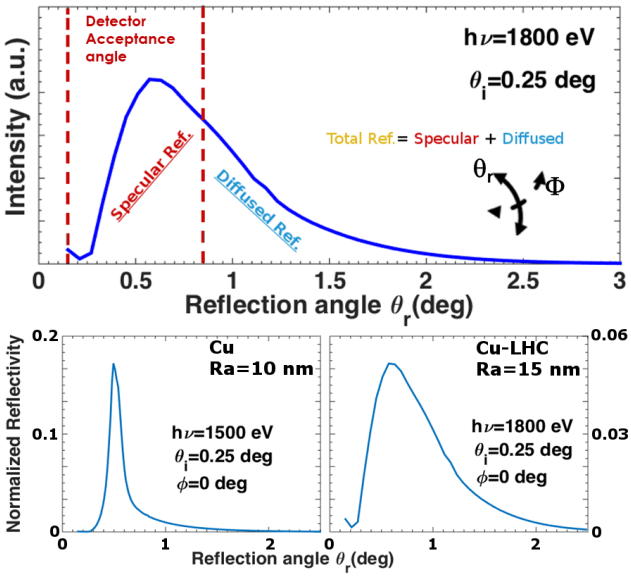

Figure 5: Total Reflectivity analysis. Top: Distinction between Specular Reflectivity area and Diffused Reflectivity during the angular scanning. Bottom: Comparison between Cu and Cu-LHC samples.

sample. The distribution presents a maximum around the geometrical specular reflection position and a tail for higher detector angular positions. The width of such distribution is correlated to the quantity of scattered radiation. Thus, R_t takes into account also this part of the reflected signal and will be calculated integrating the angular distribution. In Fig.5 bottom panel the angular distributions for Cu and Cu-LHC samples are shown. Looking at the data it is possible to conclude how lower roughness causes a reflection more focused around the $\theta_r=2\theta_i$ detector position while higher R_a are correlated to a broader distribution. However, R_t for these two samples are very similar (Table1). This result points out how the two samples reflect the same quantity of radiation but spread on different solid angle. Table 1 is a summary of the measured optical properties for a given beam energies and some incident angles.

Table 1: Optical Parameters of investigated Samples at hν=1500eV

Sample	θ_i**(deg)**	**Spec. Reflec.** ±2%	**Total. Reflec.** ±5%	**PY** ±2%
Cu	0.25°	0.61	0.74	0.18
Cu	0.5°	0.57	0.67	0.30
Cu-LHC	0.25°	0.47	0.72	0.32
Cu-LHC	0.5°	0.42	0.63	0.44
ST	0.25°	0.004	0.054	0.07
ST	0.5°	0.0017	0.006	0.06
LASE	0.25°	0.0015	0.007	0.08
LASE	0.5°	2.5e-05	0.0003	0.07

CONCLUSION

Experiments at the BESSYII OPTICS beamline allow the optical characterization of different samples of interest for FCC-hh and LHC-HL BS design. A first general analysis of the results pointed out various features to be deeper addressed in successive works [18]. Generally, the value of reflectivity used into the simulation codes is a simple average parameter obtained by analytical estimations. The experimental results demonstrate how R strongly depends on photon energy and the R(E,θ_i) function should be taken into account for the different SR emission spectra. Furthermore, it is known that roughness reduces the reflectivity of the surface. However, the simple consideration of specular reflectivity could bring, into simulations and ray tracing codes, to an underestimation of the reflected radiation due to the scattered component. In fact, for technical surfaces such component can be the dominant contribution on the total reflected radiation.

REFERENCES

[1] R. Cimino and T. Demma, "Electron cloud in accelerators," *Int. J. Mod. Phys. A*, vol. 29, no. 17, p. 1430023, 2014

[2] G. Apollinari, I. Béjar Alonso, O. Brüning, M. Lamont, and L. Rossi, "High-Luminosity Large Hadron Collider (HL-LHC): Technical Design Report V.0.1" *Cern Yellow Report:Monographs*, vol. 4, 2017.

[3] R. Kersevan, M. Ady, "Molflow+, Sinrad+", *CERN 2018, http://cern.ch/molflow*

[4] L. Boon, W. Lafayette, J. Crittenden, and K. Harkay, "Application of the SYNRAD3d Photon-Tracking Model to Shielded Pickup Measurements of Electron Clound Buildup at CesrTA," *Proceedings of IPAC2011*, pp. 5–7.

[5] R. Cimino, V. Baglin, and F. Schäfers, "Potential Remedies for the High Synchrotron-Radiation-Induced Heat Load for Future Highest-Energy-Proton Circular Colliders," *Phys. Rev. Lett.*, vol. 115, no. 26, pp. 1–5, 2015.

[6] N. Mahne et al., "Photon Reflectivity distributions from the LHC beam screen and their Implications on the Arc Beam Vacuum System," *Appl. Surf. Sci.*, vol. 235, pp. 221–226, 2004.

[7] F. Schäfers and R. Cimino, "Soft X-ray reflectivity: from quasi-perfect mirrors to accelerator walls,", *Proceedings of ECLOUD12*, 2013.

[8] V. Baglin et al., "Measurements At Epa of Vacuum and Electron-Cloud Related Effects Electron-Cloud," *Proceedings of Chamonix XI* no. September 2013, pp. 141–143, 2001.

[9] R. Cimino, V. Baglin, and I. R. Collins, "VUV synchrotron radiation studies of candidate LHC vacuum chamber materials," *Vacuum*, vol. 53, no. 1–2, pp. 273–276, 1999.

[10] R. Cimino, F. Schäfers, "Soft X-ray Reflectivity and Photoelectron Yield of technical Materials: Experimental input for instability simulations in High intensity accelerators," *Proceeding of IPAC2014*, pp. 2335–2337.

[11] R. Cimino, I. R. Collins, V. Baglin, and I. Introduction, "VUV photoemission studies of candidate Large Hadron Collider vacuum chamber materials," *Phys.Rev.Spe.Top.*, vol. 2, no. January, pp. 1–18, 1999.

[12] G. F. Dugan, K. G. Sonnad, R. Cimino, T. Ishibashi, and F. Schäfers, "Measurements of x-ray scattering from accelerator vacuum chamber surfaces, and comparison with an analytical model," *Phys. Rev. Spec. Top. - Accel. Beams*, vol. 18, no. 4, p. 040704, 2015.

[13] A. Sokolov, M. G. Sertsu, A. Gaupp, M. Luttecke, and F. Schäfers, "Efficient high-order suppression system for a metrology beamline", *J. of Synch. Rad.*, vol. 25, pp 100, 2018.

[14] A. Sokolov et al., "An XUV optics beamline at BESSY II," *Proceeding of SPIE2014*, no. February 2015, p. 92060J, 2014.

[15] Sokolov et al., "At-wavelength metrology facility for soft X-ray reflection optics," *Rev. Sci. Instrum.*, vol. 87, no. 5, 2016.

[16] R. Valizadeh, O. B. Malyshev, S. Wang, T. Sian, M. D. Cropper, and N. Sykes, "Reduction of secondary electron yield for E-cloud mitigation by laser ablation surface engineering," *Appl. Surf. Sci.*, vol. 404, pp. 370–379, 2017.

[17] F. Zimmermann, "Electron-Cloud Effects in past and future machines - walk through 50 years of Electron-Cloud studies" *ECLOUD12*, p. 9, 2013.

[18] E. La Francesca, M. Angelucci, A. Liedl, L. Spallino, L.A. Gonzalez, I. Bellafont, F. Siewert, M.G. Sertsu, A. Sokolov, F. Schäfers and R. Cimino, "Photo Reflectivity and Photoelectron Yield from Copper Technical Surfaces": to be published.